Calculation of Proton and Neutron Emission Spectra from Proton Reactions with ^{90}Zr and ^{208}Pb to 160 Mev with the GNASH Code

P.G. Young
Los Alamos National Laboratory

M.B. Chadwick
Lawrence Livermore National Laboratory
(USA)

Abstract

A number of modifications have been made to the reaction theory code GNASH in order to improve the accuracy of calculations at incident particle energies up to 200 MeV. Direct reaction and level density models appropriate for higher energy calculations are now used in the code, and most importantly, improved preequilibrium models have been incorporated into the code system. The code has been used to calculate proton-induced reactions on ^{90}Zr and ^{208}Pb for the International Code and Model Intercomparison for Intermediate Energy Reactions organized by the NEA. Calculations were performed with GNASH at incident proton energies of 25, 45, 80, and 160 MeV using both the exciton model and Feshbach-Kerman-Koonin theory for the preequilibrium component. The models and procedures used in the GNASH calculations with the exciton model are described here. The results are compared to experimental data and to the GNASH calculations with Feshbach-Kerman-Koonin theory that were provided for the code intercomparison activity.

I. Introduction

The GNASH nuclear reaction theory code has been used to support many data evaluations at incident energies below 20 MeV, including several of the ENDF/B-V and ENDF/B-VI evaluations. In recent years the code has been extended for work at higher energies and has been utilized for incident energies up to 250 MeV. In particular, it was used for comprehensive analyses of neutron-induced reactions to 40 MeV for ^{56}Fe,[1] to 50 MeV for ^{59}Co,[2] and more recently for calculations on ^{12}C, ^{16}O, ^{27}Al, ^{56}Fe, ^{59}Co, and $^{207,208}Pb$ to 200 MeV or higher.[3-7] Additionally, a preliminary set of neutron- and proton-induced transport data libraries were generated with GNASH to an incident energy of 100 MeV for ^{27}Al, ^{28}Si, ^{56}Fe, ^{184}W, and ^{238}U,[8] and similar libraries have been developed for deuteron-induced reactions to 100 MeV on ^{27}Al and ^{208}Pb.

The most recent version of the GNASH nuclear reaction theory code that has been released was described in several lectures at an ICTP workshop in Trieste in 1992.[9] Since that time several improvements have been incorporated into the code, mainly aimed at extending its capabilities for calculations at energies above 10 MeV and particularly in the preequilibrium models.[10,11] The GNASH code was used in the present calculations for proton reactions on ^{90}Zr and ^{208}Pb at energies of 25, 45, 80, and 160 MeV in support of the Nuclear Energy Agency (NEA) sponsored International Code and Model Intercomparison for Intermediate Energy Reactions.[12] Two different preequilibrium models were used in the calculations: the semiclassical exciton model of Kalbach[13] and the quantum mechanical theory of Feshbach, Kerman, and Koonin (FKK).[14] The GNASH calculations using the exciton model are described in this paper and those with FKK preequilibrium theory are described in a companion paper.[15] The exciton model calculations are compared here with experimental data and with the FKK calculations provided for the intercomparison activity.

The models and calculational procedure used in the GNASH code are described in Sec. II. In Sec. III we summarize the parameters used in the p + ^{90}Zr and ^{208}Pb calculations, and in Sec. IV we present the results of the calculations and compare them with experimental data and with the companion FKK-GNASH calculations. Finally, we give our conclusions in Sec. V.

II. Summary of Models in the GNASH Code

GNASH implements Hauser-Feshbach theory in an open-ended sequence of reaction chains, with full conservation of angular momentum.[9] Transmission coefficients for particle reactions are obtained from optical model calculations and for gamma-ray transitions from a giant resonance model.[16] In addition to providing transmission coefficients, optical model potentials are used to obtain the initial compound nucleus formation cross section, which then determines the overall normalization of all calculated emission cross sections. Continuum level densities are obtained from phenomenological level density formulations,[17] which are matched at lower excitation energies to the available discrete level data. Both the discrete and continuum structure data are utilized in the calculations.

Preequilibrium corrections become increasingly important at energies above 20 MeV and are made in standard GNASH calculations using the exciton model of Kalbach.[13] Multiple preequilibrium effects for secondary neutrons and protons are included as well as the usual corrections in the primary decay channels. The present calculations utilize a preliminary multiple preequilibrium model that was developed in the framework of the exciton model.[18] We incorporated the excitation-energy dependence of the Ignatyuk level-density formula[17] into the particle-hole state densities used in the exciton model calculations.

For actinide and heavy element studies in general, the code contains a detailed fission model, allowing use of up to three uncoupled fission barriers. The fission model was not used in the present calculations, however, because in the most relevant case (160-MeV proton reactions with ^{208}Pb), the fission contribution was relatively small compared to the neutron and proton emission cross sections.

The primary output from GNASH are absolute angle-integrated particle and gamma-ray spectra, and excitation and deexcitation cross sections of discrete states. The calculated spectra are integrated and summed to provide absolute reaction cross sections. The present configuration of the code permits the incident particle type to be neutrons, protons, deuterons, tritons, ^{3}He, or ^{4}He. In addition to gamma rays, these same particles are permitted in the decay channels. Angular effects are not included in the calculations, as the results are normally used in combination with the systematics-based parameterization of Kalbach[19] to determine angular distributions. For this purpose, the code provides tables of ratios of preequilibrium to total emission cross sections as functions of emission energy for all outgoing particles, as required in applying the Kalbach relations.

III. Description of Model Parameters in p + ^{90}Zr and p + ^{208}Pb Calculations

For both the p + ^{90}Zr and p + ^{208}Pb calculations, 35 compound nuclei were adequate to cover all significant reaction channels. Neutron, proton, deuteron, and gamma-ray emission channels were included for primary reactions with both target nuclei, and alpha-particles were added for ^{90}Zr. All reaction channels following the primary emissions were restricted to neutrons, protons, and gamma rays, with protons being included in only a few instances for the ^{208}Pb calculations. Information on discrete levels (energies, spins, parities, and branching ratios) was taken from the ENSDF nuclear structure data file for the various residual nuclei in the calculations.

For the nuclear level densities, the Ignatyuk model[17] was used in the calculations instead of other Fermi-gas models that incorporate an energy-independent level density parameter. By the use of an energy-dependent level density parameter, the Ignatyuk model includes the theoretically expected disappearance of shell effects in the nuclear level densities at higher excitation energies, such as those covered in the present calculations. Within this model the nuclear moment of inertia was given the value of the full rigid body moment of inertia. The level density parameters were chosen for each residual nucleus using the systematics of Arthur[20] and pairing corrections from Cook.[21]

Gamma-ray strength functions were calculated using the generalized Lorentzian giant resonance model of Kopecky and Uhl.[16] Giant dipole resonance parameters were obtained from the tables of Dietrich and Berman.[22] The gamma-ray strength functions were normalized so as to produce reasonable agreement with (n,γ) cross section measurements at low energies for the target nuclei.

A. Optical Model Potentials

There are a large number of global optical model potentials available for incident nucleons, and these are frequently used in GNASH calculations where accuracy requirements are only modest. However, a basic problem exists in carrying analyses to energies of 100 MeV or higher, because transmission coefficients are required in the Hauser-Feshbach calculations to low particle energies and global potentials usually do not cover such a large energy range. One method of handling this problem is to combine two potentials that span the energy region of the calculation, with particular attention to selecting a matching energy where the reaction cross sections from the two potentials are consistent.

For the ^{90}Zr calculations, we used the global proton potential of Becchetti and Greenlees[23] below 50 MeV and the Madland potential[24] at higher energies. For neutrons, the potential developed by Yamamuro[25] was used at neutron energies below 50 MeV, again with the Madland potential at higher energies. Yamamuro's potential is a combination of a lower energy potential (E < 20 MeV) that is based on systematic fits to data, and Walter and Guss's potential[26] between 20 and 50 MeV. The alpha-particle potential used by Arthur and Young[27] for calculating $^{56}Fe(n,\alpha)$ reactions was used below 50 MeV, and at higher energies the transformation prescribed by Watanabe[28] was applied to the Perey proton potential.[29] For deuterons, the potential of Perey and Perey[30] was used below 50 MeV, again with a transformed version of the Perey proton potential at higher energies.

Best results for optical model potentials are usually obtained if analyses are performed leading to potentials for the specific target nucleus and energy range under investigation. In the case of the neutron channel for the ^{208}Pb calculations, we used a coupled-channels optical model potential[31] based on experimental data in the energy range 0 to 200 MeV. To obtain the potential, the coupled-channels potential of Shamu and Young ,[32] which was developed from experimental neutron data in the energy range from 8.5 to 10 MeV, was modified and extended to both lower and higher (~ 40 MeV) energies by matching the available experimental neutron total, elastic scattering, and nonelastic scattering cross section data. Above 40 MeV, the form of the one-channel (or spherical) optical model potential of Schutt et al.[33] was used as a guide, restricted by the condition that the new potential had to be consistent with measured total and reaction cross sections. The coupled-channels code, ECIS,[34] was used with relativistic kinematics for all calculations. The potential that resulted is presented in Table I. The calculated neutron total cross section is compared with experimental data[35] and two spherical optical model potentials[33] in Fig. 1, and the reaction cross section is similarly compared[33,36] in Fig. 2. The coupled-channels potential gives a reasonable representation of the available neutron total, elastic, and nonelastic scattering cross section data to approximately 200 MeV.

For the proton channel in the p + ^{208}Pb calculations, the global potential of Becchetti and Greenlees[23] was again utilized to proton energies of 50 MeV, and the potential of Madland [24] was used at higher energies. The Perey and Perey[30] potential was utilized for deuterons, and the Watanabe transformation[28] was applied to the Perey proton potential[29] for higher energy deuterons.

B. Preequilibrium and Direct Reactions

The nuclear single-particle state densities in both the ^{90}Zr and ^{208}Pb calculations were set to A/13 MeV^{-1} in the asymptotic limit where shell effects are washed out. The matrix element normalization constants that describe the competition between precompound particle emission and internal transitions to higher exciton states in preequilibrium emission were fixed at values of 160 MeV^3 and 120 MeV^3 for the ^{90}Zr and ^{208}Pb calculations, respectively. Spin distributions for the residual states formed in preequilibrium reactions were calculated using angular momentum distributions based on the exciton model.[37]

$^{208}Pb(p,p')$ direct reaction cross sections were included in the GNASH calculations under the assumption that they were identically equal to (n,n') values calculated from the coupled-channels potential described in the previous section. For the (n,n') calculations, one-phonon excitations were assumed for the discrete ^{208}Pb states at 2615 (3^-), 4085 (2^+), 4323 (4^+), 4424 (6^+), and 4610 (8^+) keV, plus a cluster of low-energy octupole resonance (LEOR) states represented by a single 3^- state at 5380 keV. Deformation parameters were taken from DWBA analyses of proton-induced measurements for the states below 5-MeV excitation energy, and the deformation for the LEOR state at 5380 keV was scaled from the 3^- state at 2615 keV.

Table 1. Deformed optical model potential for ^{208}Pb + n calculations over the neutron energy range 1 keV ≤ E_n ≤ 200 MeV

Well Depth (MeV)		Geometry (fm)	
$V_R = 50.04 - 0.279\ E_n$	[0 < E_n < 60 MeV]	$r_R = 1.183$	$a_R = 0.6966$
$= 111.0925 - 19\ \ln(E_n)$	[60 ≤ E_n ≤ 200 MeV]		
$W_d = 1.00 + 0.2502\ E_n$	[0 < E_n < 14 MeV]	$r_R = 1.273$	$a_R = 0.699$
$= 5.722 - 0.08705\ E_n$	[14 ≤ E_n ≤ 65.7 MeV]		
$= 0$	[65.7 ≤ E_n ≤ 200 MeV]		
$W_V = 0$	[0 < E_n < 14.4 MeV]	$r_R = 1.273$	$a_R = 0.699$
$= -2.60 + 0.18\ E_n$	[14.4 ≤ E_n ≤ 40 MeV]		
$= 2.20 + 0.06\ E_n$	[40 ≤ E_n ≤ 100 MeV]		
$= 8.20$	[100 ≤ E_n ≤ 200 MeV]		
$V_{SO} = 6.18$	[0 < E_n < 200 MeV]	$r_R = 1.16$	$a_R = 0.677$

IV. Comparison of Calculated Results with Experimental Data

The results of the calculations are compared with experimental data in this section. In most of the illustrations both the calculations using the exciton preequilibrium model (dashed curves) and the FKK preequilibrium model (solid curves) are included for comparison.

The angle-integrated neutron emission spectra from p + ^{90}Zr reactions with E_p = 25, 45, 80, and 160 MeV are compared with experimental data[38-40] in Figs. 3 - 6. The Hauser-Feshbach and multiple preequilibrium components that accompanied the FKK theory and exciton model calculations are also illustrated on the figures. Both the FKK and exciton models give good representations of the measurements, with the FKK calculation being slightly preferred at 25 and 160 MeV and the exciton model calculations reproducing the data marginally better at 45 and 80 MeV. The multiple preequilibrium component to the neutron emission is negligible at 25 MeV, becomes significant at 45 MeV, and then gets to be increasingly important at higher energies. The Hauser-Feshbach component dominates the neutron emission spectra at lower emission energies but becomes negligible at the higher emission energies at each incident energy.

Calculated and measured[41] angular distributions of neutrons emitted at 20 and 30 MeV from 45-MeV protons on ^{90}Zr are shown in Fig. 7 . Similar comparisons with experimental data[39] are illustrated in Fig. 8 for 80-MeV protons incident on ^{90}Zr with emitted neutron energies of 22, 42, and 62 MeV, and in Fig. 9 for emitted protons[42] at proton energies of 20, 40, and 60 MeV. And, angular distributions of neutron emission at 80, 100, and 140 MeV for 160-MeV protons on ^{90}Zr are compared to measurements[40] in Fig. 10. A general feature seen in all cases is that the angular distributions are better described at backward angles by the Kalbach systematics as compared to the FKK calculations. The difference in the two calculations is greatest for emitted neutrons, but the general trend of higher angular distributions from the Kalbach systematics at back angles is still seen for proton emission in Fig. 9, with slightly improved agreement with measurements.

The angle-integrated neutron emission spectra from p + ^{208}Pb reactions at E_p = 45 and 80 MeV are shown with experimental data[38,39] in Figs. 11 and 12. Figure 13 illustrates the neutron angular distributions at neutron emission energies of 37, 54, and 70 MeV for 80-MeV incident protons on ^{208}Pb with measurements.[39] The angle-integrated neutron emission spectrum[40] for 160-MeV protons on ^{208}Pb is shown in Fig. 14, and neutron emission spectra[40] at laboratory angles of 11°, 69°, and 145° are given in Fig. 15 for the 160-MeV incident proton case. The comparisons of experimental data with calculations for the p + ^{208}Pb reactions have the same general characteristics as is seen in the p + ^{90}Zr comparisons. In particular, the angle-integrated spectra for the calculations with both the exciton and FKK preequilibrium models agree satisfactorily with the angle-integrated data, but the angular distributions obtained by combining the exciton preequilibrium model calculations with the Kalbach systematics[19] reproduce the measurements better at backward angles than do the pure FKK calculations. This feature is well illustrated by the 145° neutron emission spectrum for 160-MeV protons incident on ^{208}Pb in Fig. 15.

Finally, to illustrate the general consistency of these calculations with experimental data, we compare high-resolution measurements[31] of gamma-ray production cross sections for individual gamma rays in n + ^{208}Pb reactions with GNASH calculations made with the same models and essentially the same parameters. In particular, the measured data for the 570-keV and 1026-keV gamma rays from the ^{208}Pb(n,2nγ)^{207}Pb and ^{208}Pb(n,9nγ)^{200}Pb reactions are compared in Figs. 16 and 17 with the calculations, both with and without the multiple preequilibrium contributions.

These comparisons show relatively good agreement between the calculations and the experimental data, and illustrate the importance of including multiple preequilibrium effects in the calculations.

V. Conclusions

The calculations with the GNASH code of neutron and proton emission data for incident protons of energy between 25 and 160 MeV on ^{90}Zr and ^{208}Pb targets give satisfactory agreement with experimental data for the models and parameters chosen. We find that both the exciton model and FKK theory provide preequilibrium contributions that are consistent with angle-integrated emission spectra. The angular distributions that are obtained using FKK theory fall off somewhat too rapidly relative to the experimental data at backward angles, especially for emitted neutrons, whereas angular distributions obtained by combining the systematics of Kalbach[19] with the exciton model agree reasonably with measurements at all angles. We find that multiple preequilibrium contributions are important in calculations at higher energies, especially in determining individual reaction components such as discrete gamma-ray cross sections.

From our study we conclude that the best procedure to follow when providing evaluated data at higher energies from the GNASH code system is to combine FKK-GNASH calculations of angle-integrated spectra with standard GNASH calculations using Kalbach systematics to obtain the energy-angle correlations in the data. In this way the greater predictive power of FKK theory is coupled with somewhat more reliable angular distribution estimates from the systematics of a large body of experimental data. We plan to make the present version of the GNASH code system available from the NEA Data Bank in the near future.

VI. Acknowledgments

We wish to thank Marshall Blann for suggesting that we participate in this model code intercomparison activity and for several useful discussions. This work was performed in part under the auspices of the U.S. Department of Energy by Los Alamos National Laboratory under contract No. W-7405-Eng-36 and by Lawrence Livermore National Laboratory under contract No. W-7405-Eng-48.

References

1. E. D. Arthur and P. G. Young, "Evaluation of Neutron Cross Sections to 40 MeV for $^{54,56}Fe$," Proc. Sym. on *Neutron Cross Sections from 10 to 50 MeV*, Brookhaven National Laboratory, Upton, N.Y., 12-14 May 1980, BNL-NCS-51245 (1980), v. II, p. 731, and LA-8626-MS (1980).

2. E. D. Arthur, P. G. Young, and W.K. Matthes, "Calculation of ^{59}Co Neutron Cross Sections between 3 and 50 MeV," Proc. Sym. on *Neutron Cross Sections from 10 to 50 MeV*, Brookhaven National Laboratory, Upton, N.Y., 12-14 May 1980, BNL-NCS-51245 (1980), v. II, p. 751.

3. M. B. Chadwick, M. Blann, G. Reffo, and P. G. Young, "Model Calculations of Nuclear Data for Biologically-Important Nuclei," Proc. International Conference on *Nuclear Data for Science and Technology*, 9-13 May 1994, Gatlinburg, Tennessee, USA, to be published.

4. H. Hitzenberger, A. Pavlik, H. Vonach, R. C. Haight, R. O. Nelson, and P. G. Young, "Study of ^{27}Al (n,$x\gamma$) Reaction up to E_n = 400 MeV," *ibid.*

5. S. M. Sterbenz, F. B. Bateman, T. M. Lee, R. C. Haight, P. G. Young, M. B. Chadwick, R. C. Goeckner, C. E. Brient, S. M. Grimes, H. Vonach, and P. Maier-Komor, "The $^{56}Fe(n,x\alpha)$ Reaction from Threshold to 30 MeV," *ibid.*

6. R. C. Goeckner, S. M. Grimes, C. E. Brient, T. M. Lee, S. M. Sterbenz, F. B. Bateman, R. C. Haight, P. G. Young, M. B. Chadwick, O. Wasson, and H. Vonach, "The $^{59}Co(n,\alpha)$ Reaction from Threshold to 30 MeV," *ibid.*

7. A. Pavlik, H. Vonach, M. B. Chadwick, R. C. Haight, S. A. Wender, P. G. Young, "$^{207,208}Pb(n,xn\gamma)$ Reactions for Neutron Energies up to 200 MeV," *ibid.*

8. P. G. Young, E. D. Arthur, M. Bozoian, T. R. England, G. M. Hale, R. J. LaBauve, R. C. Little, R. E. MacFarlane, D. G. Madland, R. T. Perry, and W. B. Wilson, "Transport Data Libraries for Incident Proton and Neutron Energies to 100 MeV," *Trans. Amer. Nucl. Soc.* **60**, 271 (1989), and LA-11753-MS (1990).

9. P. G. Young, E. D. Arthur, and M. B. Chadwick, "Comprehensive Nuclear Model Calculations: Introduction to the Theory and Use of the GNASH Code," Proc. ICTP Workshop on *Comp. and Anal. of Nucl. Data Relevant to Nucl. En. and Safety*, 10 Feb. - 13 Mar., 1992, Trieste, Italy; *ibid*, Los Alamos National Laboratory report LA-12343-MS (1992).

10. P. G. Young, M. B. Chadwick, and M. Bozoian, "Use of the Nuclear Model Code GNASH to Calculate Cross Section Data at Energies up to 100 MeV," Proc. Sym. on *Nuclear Data Evaluation Methodology*, Upton, NY, 12-16 October 1992, (Ed. C. L. Dunford, World Scientific Press, Singapore, 1993) p. 480.

11. P. G. Young and M. B. Chadwick, "Improvements to the Nuclear Model Code GNASH for Cross-Section Calculations at Higher Energies," Proc. International Conference on *Nuclear Data for Science and Technology*, 9-13 May 1994, Gatlinburg, Tennessee, USA, to be published.

12. M. Blann and P. Nagel, "International Code and Model Intercomparison for Intermediate Energy Reactions," Nuclear Energy Agency Document NEA/NSC/DOC(92)1, 1992.

13. C. Kalbach, *Z. Phys. A* **283**, 401 (1977).

14. H. Feshbach, A. Kerman, and S. Koonin, *Ann. Phys. (N.Y.)* **125**, 429 (1980).

15. M. B. Chadwick and P. G. Young, "FKK-GNASH Calculations of (*p,xn*) and (*p,xp*) Reactions on ^{90}Zr and ^{208}Pb for NEA Code Intercomparison," International Code Intercomparison, LA-UR-93-104 (1993): M. B. Chadwick and P. G. Young, "Progress in Applying the FKK Multistep Reaction Theory to Intermediate Energy Nuclear Data," present Conference.

16. J. Kopecky and M. Uhl, "Test of Gamma-Ray Strength Functions in Nuclear Reaction Model Calculations," *Phys. Rev. C* **42**, 1941 (1990).

17. A. V. Ignatyuk, G. N. Smirenkin, and A. S. Tishin, *Sov. J. Nucl. Phys.* **21**, 255 (1975).

18. M. B. Chadwick, H. M. Blann, P. G. Young and D. C. George, "Multiple Preequilibrium Processes in FKK Theory," submitted *Phys. Rev. C* (1994).

19. C. Kalbach, *Phys. Rev. C* **37**, 2350 (1988).

20. E. D. Arthur: page 10 of LA-1173-MS in Ref. 9.

21. J. Cook et al., *Aust.J.Phys.* **20**,477(1967)

22. S. S. Dietrich and B. L. Berman, "Atlas of Photoabsorption Cross Sections Obtained with Monoenergetic Photons," *Atomic Data and Nuclear Data Tables* **38**, 199 (1988).

23. F. D. Becchetti, Jr., and G. W. Greenlees, *Phys. Rev.* **182**, 1190 (1969).

24. D. G. Madland, "Recent Results in the Development of a Global Medium-Energy Nucleon-Nucleus Optical-Model Potential," Proc. Specialists' Meeting on Preequilibrium Nuclear Reactions, Semmering, Austria, 10-12 February 1988 [NEANDC-245 'U' (1988)] p.103.

25. N. Yamamuro, "Nuclear Cross Section Calculations with a Simplified-Input Version of ELIESE-GNASH Joint Program," Proc. Int. Conf. on *Nucl. Data for Sci. and Tech.,* Mito (1988) p.489, and JAERI-M 90-006 (1990).

26. R. L. Walter and P. P. Guss, "A Global Optical Model for Neutron Scattering for A > 53 and 10 MeV < E < 80 MeV," Proc. Int. Conf. on Nuc.Data for Basic and Applied Science, Santa Fe (1985) p.1079.

27. E. D. Arthur and P. G. Young, "Evaluated Neutron-Induced Cross Sections for 54,56Fe to 40 MeV," Los Alamos National Laboratory report LA-8626-MS (1980).

28. H. Watanabe, Nucl. Phys. 8, 484 (1958).

29. F. G. Perey, Phys. Rev. 131, 745 (1963).

30. C. M. Perey and F. G. Perey, Phys. Rev. 132, 755 (1963).

31. H. Vonach, A. Pavlik, M. B. Chadwick, R. C. Haight, R. O. Nelson, S. A. Wender, and P. G. Young, "^{207,208}Pb(n,xng) Reactions for Neutron Energies up to 200 MeV," submitted *Phys. Rev. C* (1994).

32. R. E. Shamu and P. G. Young, "Coupled-Channels Optical-Model Analysis of n-208Pb Scattering at Low Energies," *Phys. G: Nucl. Part. Phys.* **19**, L169 (1993); see also P.G. Young and R.E. Shamu, "Methods in Coupled-Channel Optical Model Analysis of n - ^{208}Pb Scattering at Low Energies," Proc. Sym. on *Nuclear Data Evaluation Methodology,* Upton, NY, 12-16 October 1992, (Ed. C. L. Dunford, World Scientific Press, Singapore, 1993) p. 360.

33. R. L. Schutt, R. E. Shamu, P. W. Lisowski, M. S. Moore, and G. L. Morgan, *Phys. Lett. B* **203**, 22 (1988); see also R. W. Finlay, J. R.M. Annand, T. S. Cheema, and J. Rapaport, *Phys. Rev. C* **30**, 796 (1984).

34. J. Raynal, "Optical Model and Coupled-Channel Calculations in Nuclear Physics," International Atomic Energy Agency report IAEA SMR-9/8 (1972) p. 281.

35. P. W. Lisowski, G. F. Auchampaugh, M. S. Moore, G. L. Morgan, and R. E. Shamu, "Neutron Cross Section Measurements at WNR," Proc. Sym. on *Neutron Cross Sections from 10 to 50 MeV*, 12-14 May 1980, Brookhaven National Laboratory, BNL-NCS-51245 (1980) p. 301; R. Haight, R. Finlay, et al., personal communication (1992).

36. Experimental data obtained from the National Nuclear Data Center, Brookhaven National Laboratory, Upton, New York.

37. M. B. Chadwick, P. G. Young, P. Oblozinsky, and A. Marcinkowski, "Preequilibrium Spin Effects in Feshbach-Kerman-Koonin and Exciton Models and Application to High-Spin Isomer Production," to be published in *Phys. Rev. C* (1994).

38. M. Blann, R. R. Doering, A. Galonsky, D. M. Patterson, and F. E. Serr, Nucl. Phys. A257, 15 (1976).

39. A. Galonsky, R. R. Doering, D. M. Patterson, and H. W. Bertini, Phys. Rev. C 14, 748 (1976).

40. M. Trabandt, W. Scobel, M. Blann, B. A. Pohl, R. C. Byrd, C. C.Foster, and R. Bonetti, Phys. Rev. C 39, 452 (1989).

41. A. A. Cowley, A. van Kent, J. J. Lawrie, S. V. Fortsch, D. M. Whittal, J. V. Pilcher, F. D. Smit, W. A. Richter, R. Lindsay, I. J. van Heerden, R. Bonetti, and P. E. Hodgson, Phys. Rev. C 43, 678 (1991).

42. W. Scobel, M. Trabandt, M. Blann, B. A. Pohl, B. R. Remington, R. C. Byrd, C. Foster, R. Bonetti, C. Chiesa, and S. M. Grimes, *Phys. Rev. C* **41**, 2010 (1990).

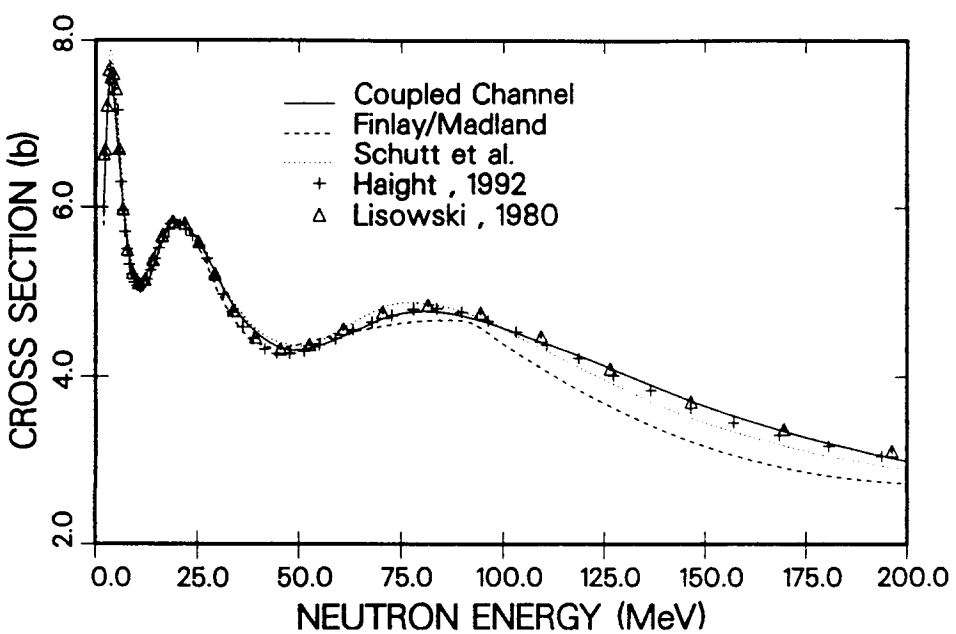

Fig. 1. Calculated and measured[35] neutron total cross section for ^{208}Pb. The dashed and dotted curves were calculated with the optical model potentials in Ref. 33.

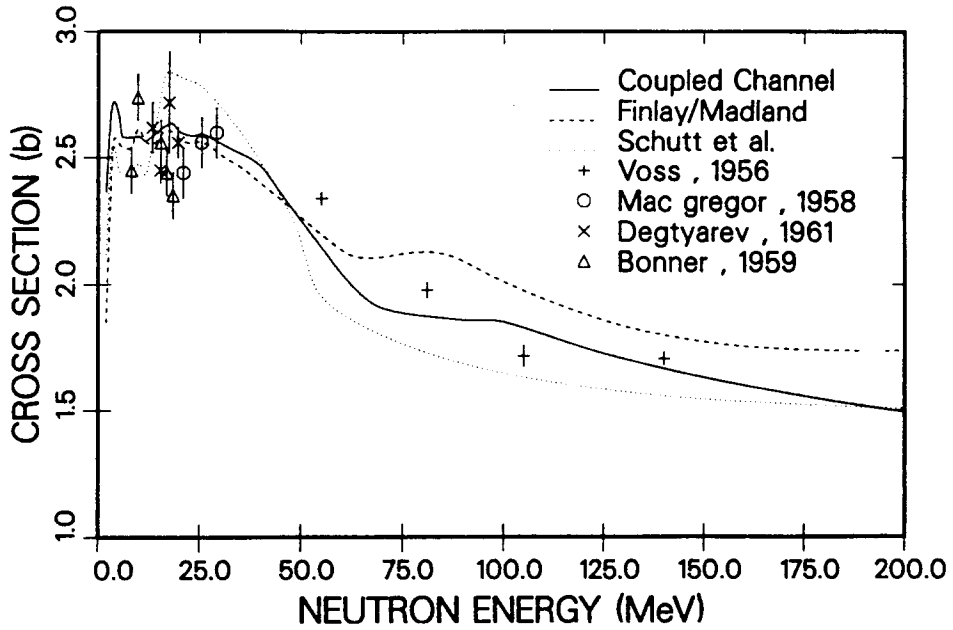

Fig. 2. Calculated and measured[36] neutron reaction cross section for ^{208}Pb. The dashed and dotted curves were calculated with the optical model potentials in Ref. 33.

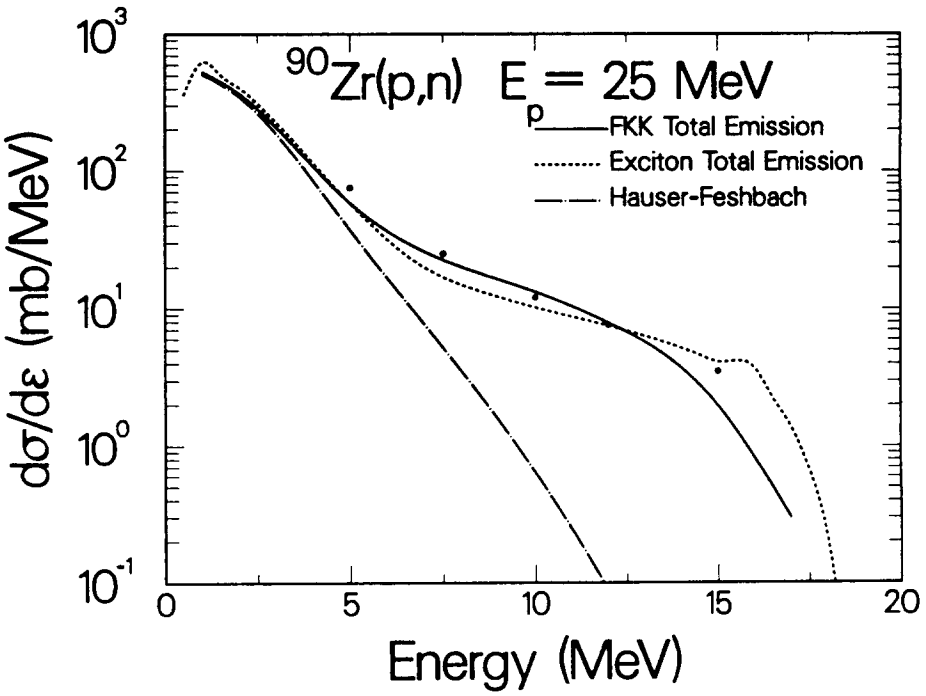

Fig. 3. Angle-integrated neutron emission spectrum from 25-MeV proton bombardment of ^{90}Zr. The experimental data are from Ref. 38.

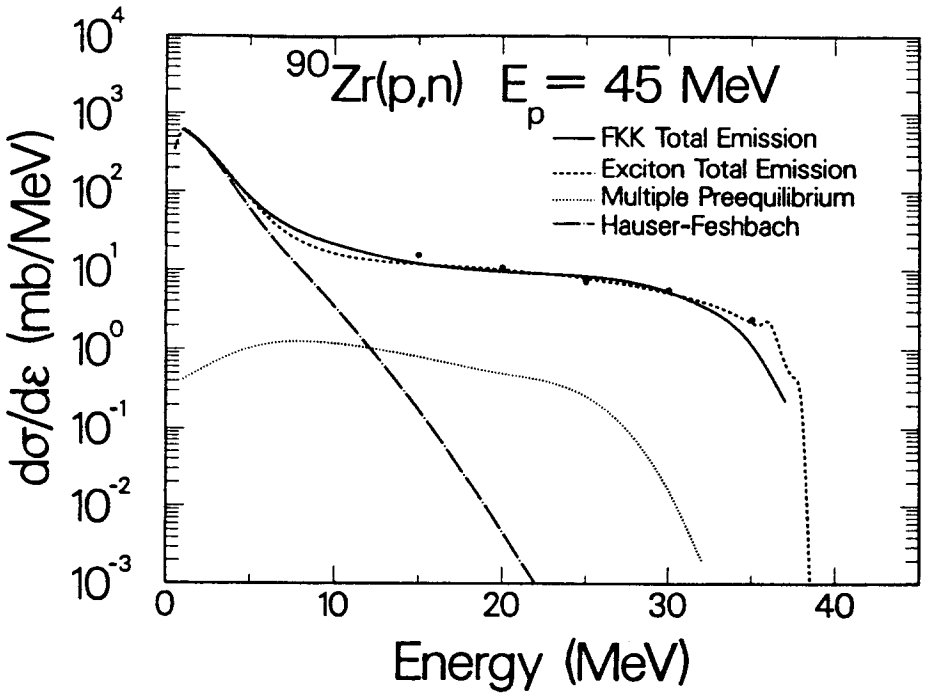

Fig. 4. Angle-integrated neutron emission spectrum from 45-MeV proton bombardment of ^{90}Zr. The experimental data are from Ref. 38.

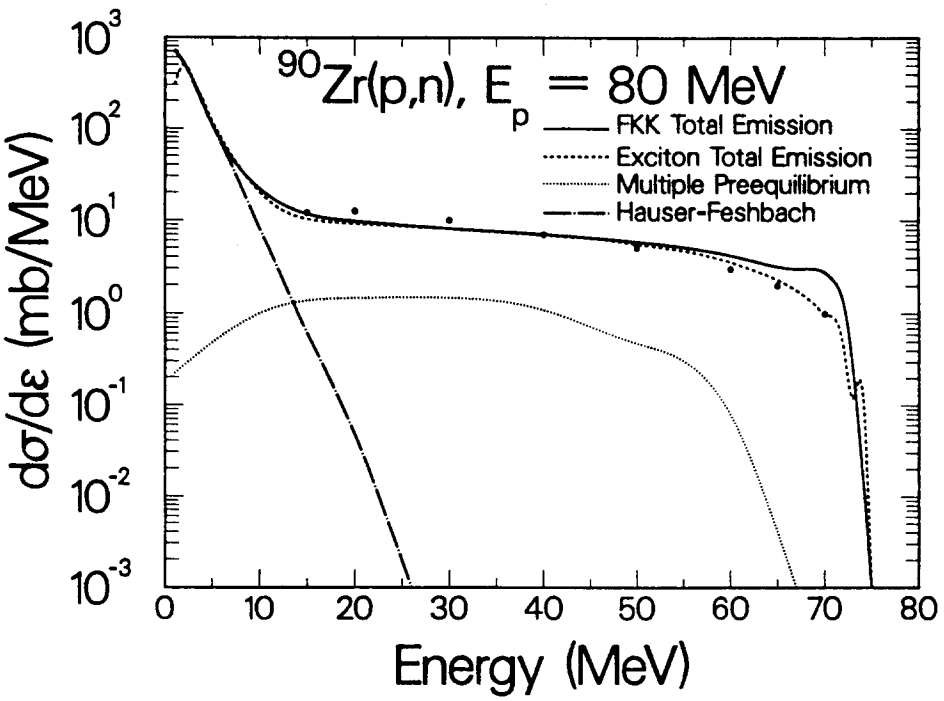

Fig. 5. Angle-integrated neutron emission spectrum from 80-MeV proton bombardment of ^{90}Zr. The experimental data are from Ref. 39.

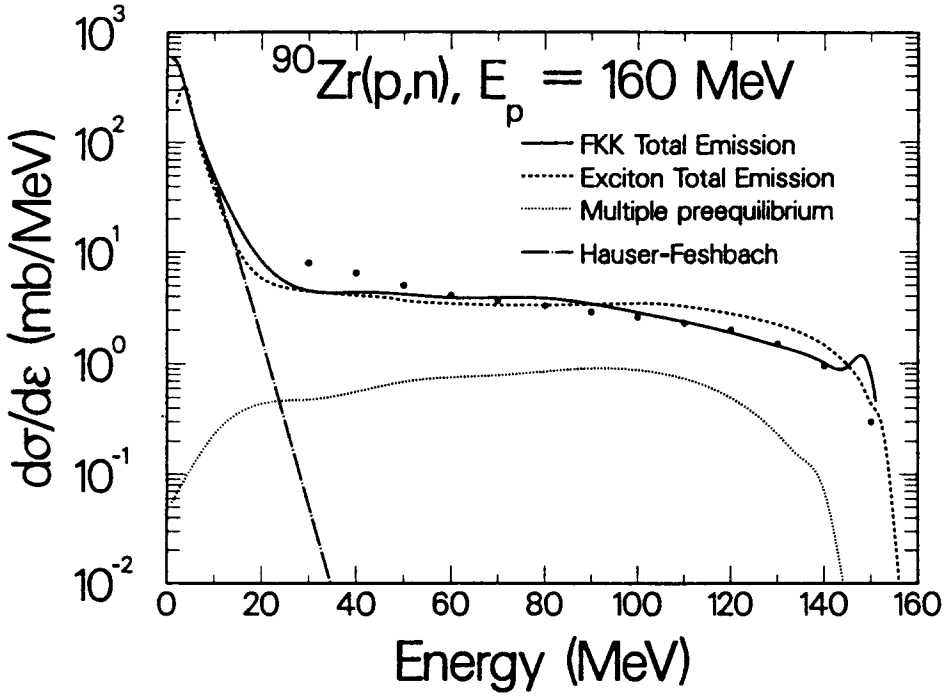

Fig. 6. Angle-integrated neutron emission spectrum from 160-MeV proton bombardment of ^{90}Zr. The experimental data are from Ref. 40.

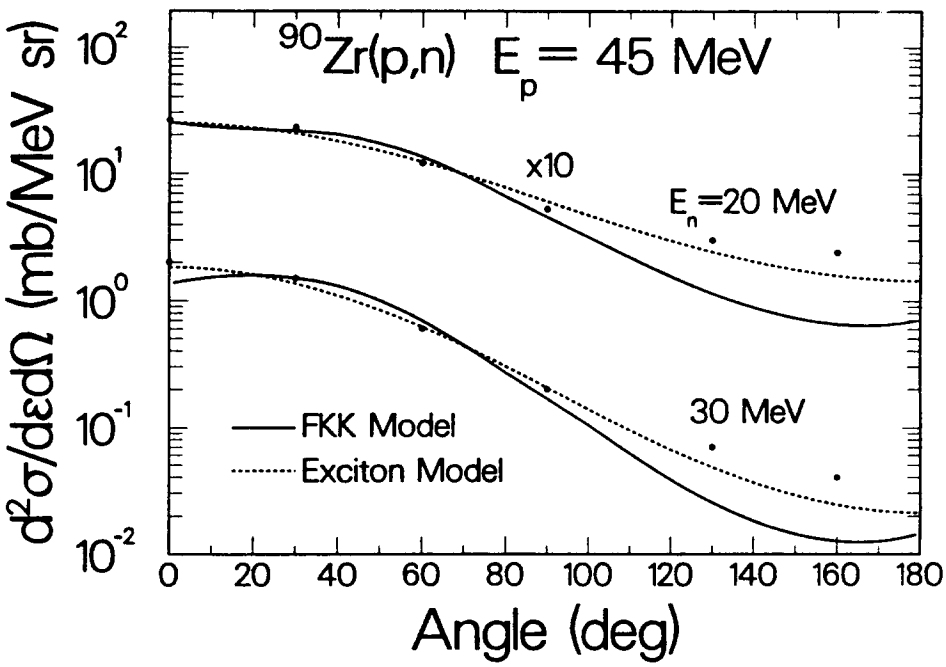

Fig. 7. Neutron angular distributions at emission energies of 20 and 30 MeV from 45-MeV proton bombardment of ^{90}Zr. The experimental data are from Ref. 41.

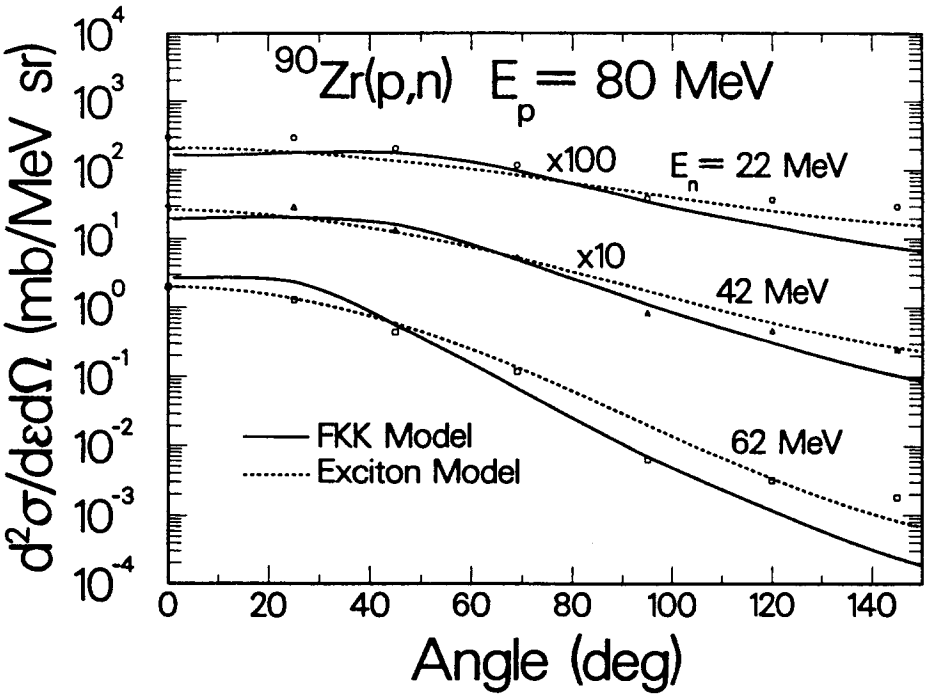

Fig. 8. Neutron angular distributions at emission energies of 22, 42, and 62 MeV from 80-MeV proton bombardment of ^{90}Zr. The experimental data are from Ref. 39.

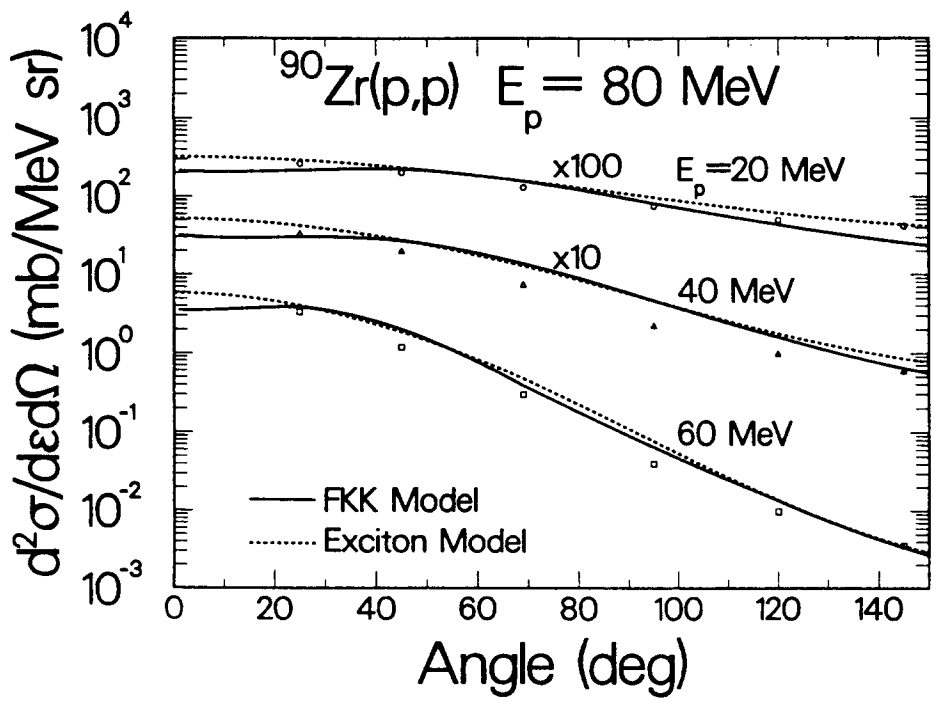

Fig. 9. Proton angular distributions at emission energies of 20, 40, and 60 MeV from 80-MeV proton bombardment of ^{90}Zr. The experimental data are from Ref. 42.

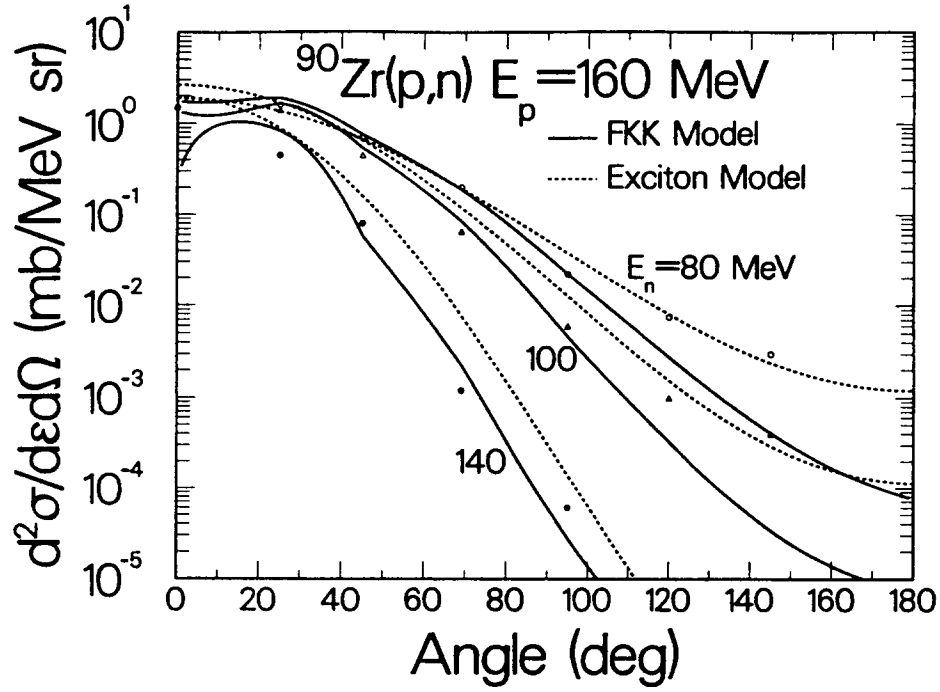

Fig. 10. Neutron angular distributions at emission energies of 80,100, and 140 MeV from 160-MeV proton bombardment of ^{90}Zr. The experimental data are from Ref. 40.

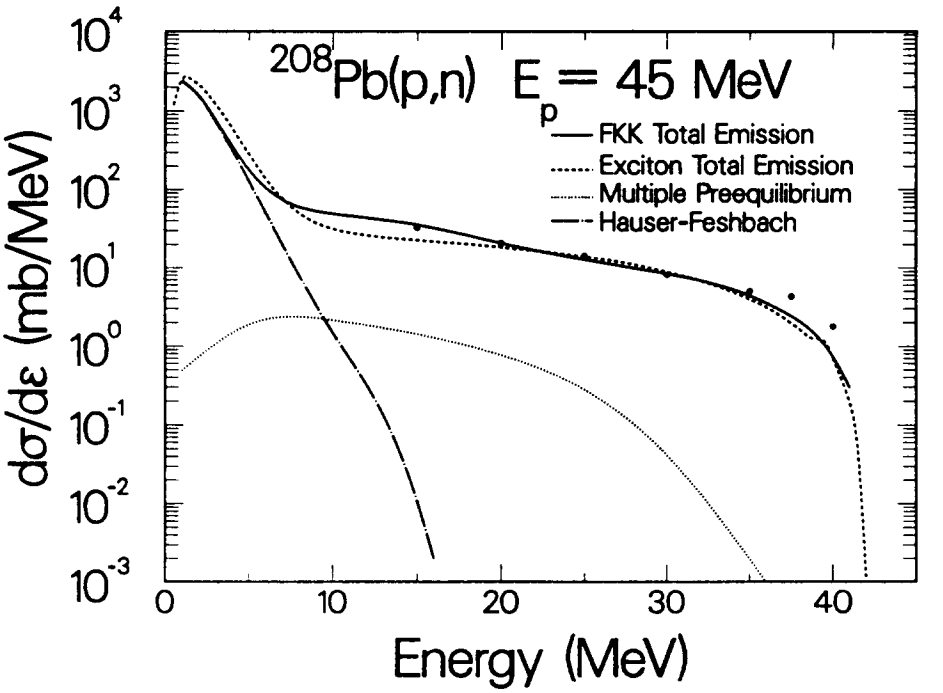

Fig. 11. Angle-integrated neutron emission spectrum from 45-MeV proton bombardment of ^{208}Pb. The experimental data are from Ref. 38.

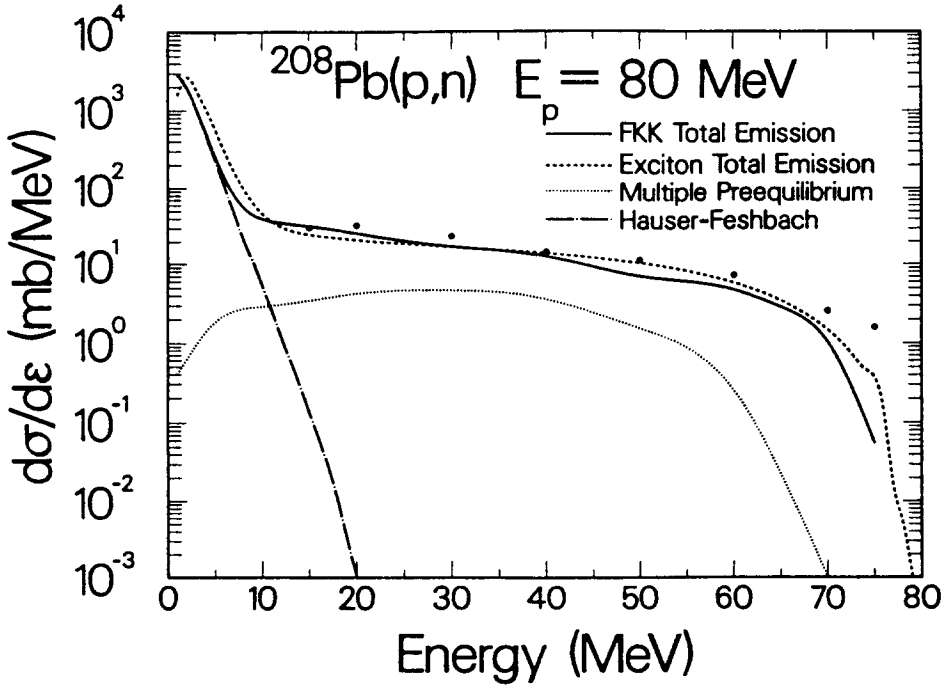

Fig. 12. Angle-integrated neutron emission spectrum from 80-MeV proton bombardment of ^{208}Pb. The experimental data are from Ref. 39.

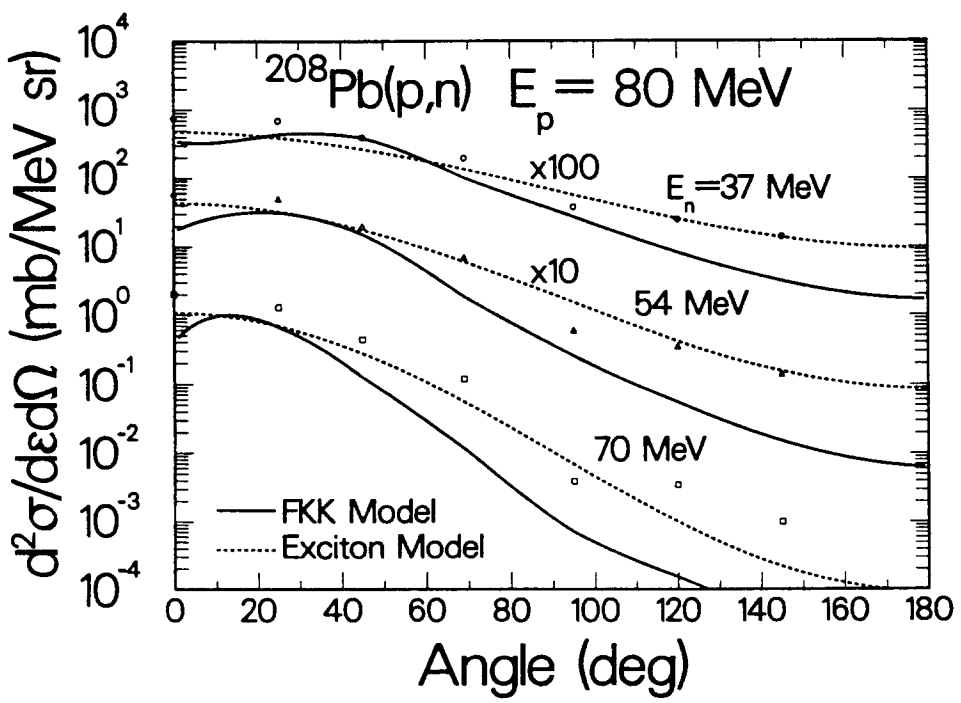

Fig. 13. Neutron angular distributions at emission energies of 37, 54, and 70 MeV from 80-MeV proton bombardment of ^{208}Pb. The experimental data are from Ref. 39.

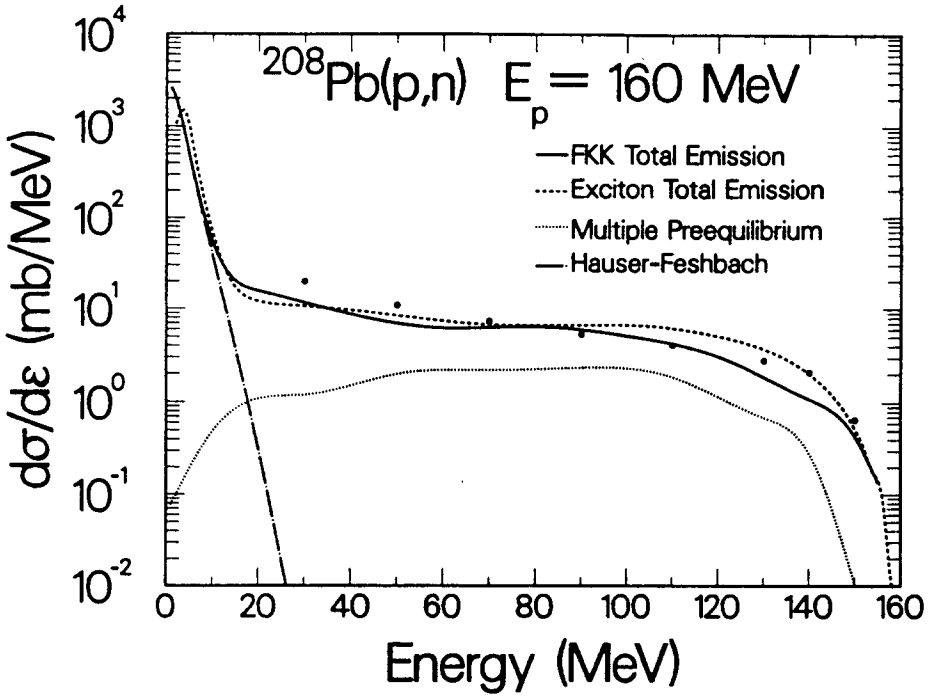

Fig. 14. Angle-integrated neutron emission spectrum from 160-MeV proton bombardment of ^{208}Pb. The experimental data are from Ref. 40.

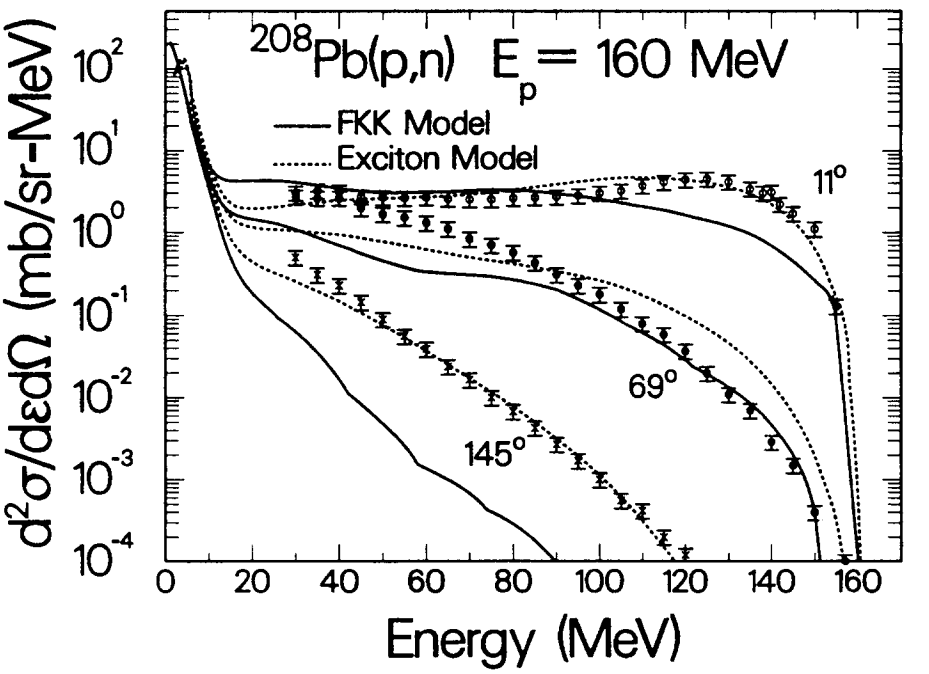

Fig. 15. Neutron emission spectrum at laboratory angles of 11°, 69°, and 145° from 160-MeV proton bombardment of ^{208}Pb. The experimental data are from Ref. 40.

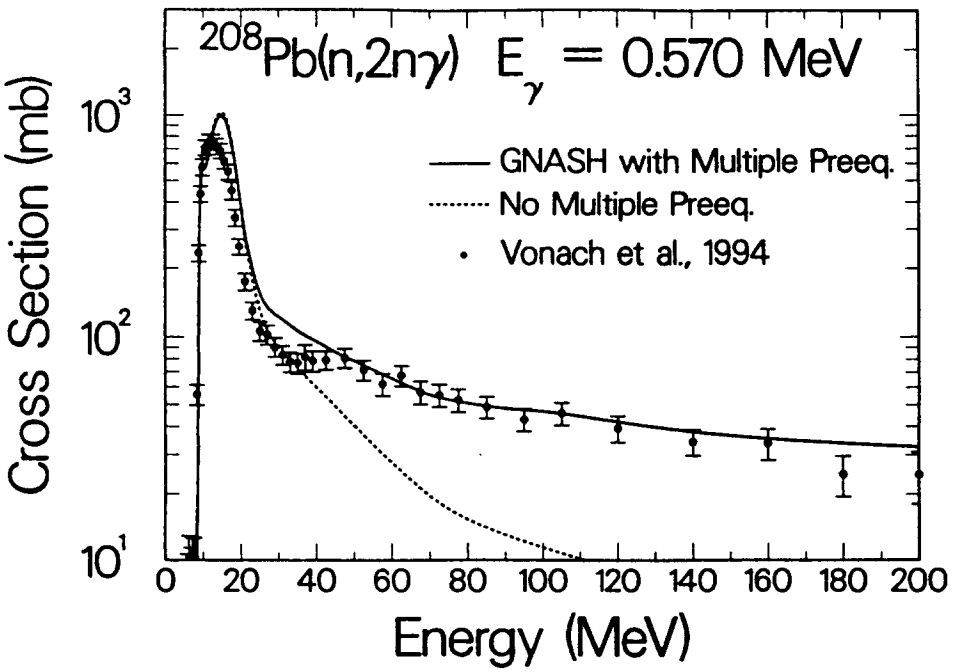

Fig. 16. Calculated and measured[31] cross sections for production of the 0.570-MeV gamma ray from the ^{208}Pb(n,2nγ) reaction.

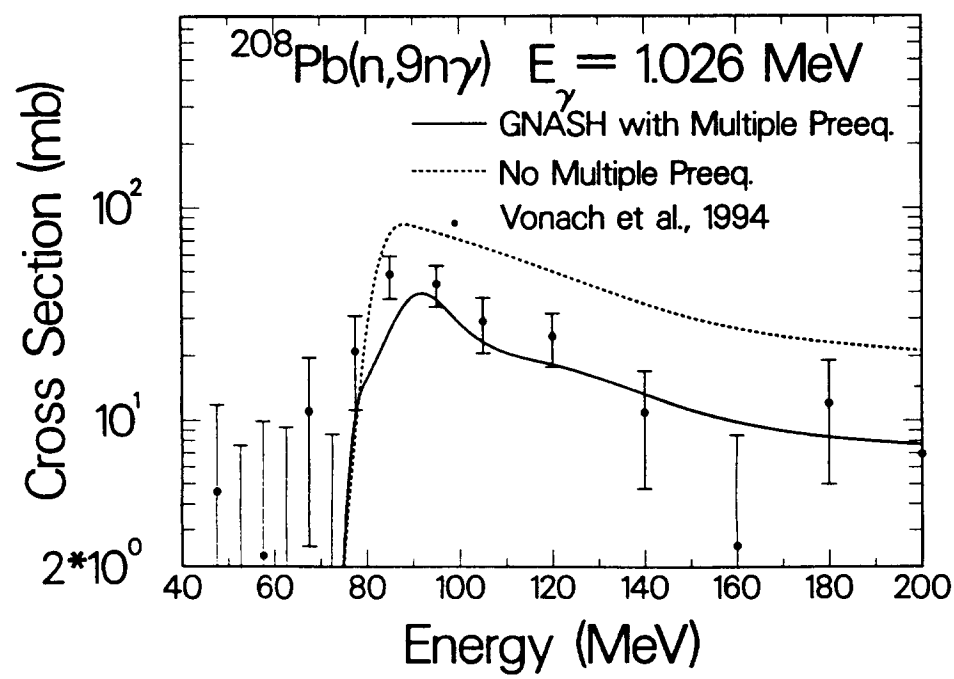

Fig. 17. Calculated and measured[31] cross sections for production of the 1.026-MeV gamma ray from the ^{208}Pb(n,9nγ) reaction.